FIBER-MATRIX SEPARATION IN RIBBED SMC AND BMC PARTS

Sari K. Christensen, Bryan Hutchinson,
Esther M. Sun, and Tim A. Osswald
Polymer Processing Research Group
University of Wisconsin-Madison
Madison, WI

Bruce A. Davis
The Madison Group: PPRC
Madison, WI

Abstract

A well known, and widely ignored fact, is that fiber reinforced parts have large variations in fiber density due to fiber-matrix separation induced during processing. Fiber-matrix separation leads to ribs with poor fiber content, and resin rich edges in large parts, weakening the structural integrity of the product. The resin rich areas on the cosmetic side of a ribbed fiber reinforced part are the main contributor of sink-mark formation. Within this research, a non-Newtonian, non-isothermal finite element flow model is developed to study the flow processes that take place during mold filling of SMC and BMC parts with integrated ribs. It was found that the flow resistance into the rib reflects itself through a pressure drop at the rib entrance. Based on this pressure loss we predict an increase of resin flow out of the fiber bed at the rib entrance or at a flow obstruction which leads to varying fiber density distribution throughout the part. Using dimensional analysis we developed a nomogram that relates rib and part geometry to head loss at the entrance of the rib, and consequently, to fiber-matrix separation. The fiber density distribution was measured in fiber reinforced unsaturated polyester parts using burn-out techniques. Both, predicted and experimental results showed a reduced fiber density content inside ribs and around sharp corners.

Introduction

The most significant contributions of reinforced thermoset composites include weight reduction, heat resistance and higher toughness. The demands of recent applications combine both structural and cosmetic requirements. The presence of integrated ribs in finished components fabricated from sheet molding compound (SMC) or bulk molding compound (BMC) provides the necessary rigidity, however, at the same time causes some degree of deformation on the cosmetic surface. These deformations, known as sink-marks, result from material inhomogeneties arising from flow induced fiber orientation, fiber-matrix separation, curing, polymerization shrinkage and processing conditions. Fiber-matrix separation in parts with ribbed substructures was measured by Jutte in the early 1970s [1], who also measured its effect on sink-mark formation. Sun [2] predicted similar tendencies in sink-mark formation using numerical models. Some of her results are reported in this paper. Osswald [3] measured pressure drops at rib entrances. Michaeli and Semmler [4], also report measured pressure losses at rib and boss entrances in fiber reinforced parts. This paper presents a model that can be used to predict fiber-matrix separation in parts with ribbed substructures.

Mold Filling

Experimental evidence of the flow front progression in compression molded parts with substructures has shown that the filling is preferential to the planar direction. Thus the filling into ribs and bosses is delayed until the pressure above these regions reaches a critical level. A simulation program was developed to simulate the flow into ribs. The effect of the flange and rib dimensions on the flow rate and flow resistance into the ribs is also examined. Since the ribbed section is symmetric, only half of the domain is calculated. The dimension and boundary conditions used in the simulation are shown in Fig. 1. The closing velocity is assigned a value of 0.4 mm/s with an open flow front condition at the end of the rib and flange. The other edges are assumed to have a no slip boundary condition. The mold temperature is set to 150°C and the charge temperature is set at 20°C.

The temperature field at the beginning of compression shows that the outer layers have quickly reached the mold temperature, while most of the core still remains at the charge temperature. The higher resin temperatures at the mold walls act as a lubricating layer due to the temperature dependent viscosity. The corresponding velocity field shows high velocity gradients near the mold surfaces which are due to the high viscosity gradients. Fountain flow effect were also apparent in the simulation results due to the no slip boundary condition applied at the mold surfaces.

The pressure distribution showed that the lowest pressure is at the end of the flange and at the end of the rib because of the flow front boundary condition. The highest pressure gradients are near the junction of the rib and flange, thus indicating that for the material to flow into the rib, a significant amount of pressure is required. When plotting the pressure distribution (Fig. 2), a parabolic distribution in the flange area (right side of the figure) and a linear pressure drop in the rib area (left side of the figure) is apparent. The location of the pressure points within the flange and rib are shown in Fig. 3. Here the junction between the flange and the rib is denoted as the reference point "0". Of particular interest is the pressure drop at the

rib entrance. Here, the pressure difference is computed from the extensions of the parabolic and linear pressure curves representing the flange and rib profiles. Experimental data from Osswald [3] confirms the pressure loss at the rib entrance. It is proposed that this pressure drop, required to force the material into the rib, is the driving force in fiber-matrix separation.

Through dimensional analysis, the influence of the geometric and processing parameters on the system can be determined. The Buckingham Π theorem is used to generate sets of dimensionless groups without making reference to the differential equations. The three dimensionless parameters can be grouped as follows:

$$\Pi_1 = \frac{\Delta P\, H}{\eta\, \dot{h}} \tag{1}$$

$$\Pi_2 = \frac{L}{H} \tag{2}$$

$$\Pi_3 = \frac{R}{H} \tag{3}$$

The first group Π_1 indicates the ratio of the pressure force to viscous force. This group contains the information which controls the flow resistance into the ribs. The second and third group, Π_2 and Π_3, involve the geometric parameters which indicate the influence of the rib design. The relationship of these three groups was found using the flow simulation program. Figure 4 shows the plot of Π_1 as a function of Π_2 and Π_3. The figure shows that the larger the rib thickness, the easier the flow into the ribs. However, a small lead-in radius will reduce the flow or increase the resistance into the ribs (Π_3). High pressure loss at the entrance of the rib is due to viscous friction (Π_1). This pressure loss will result in fiber-matrix separation in these areas which in turn will weaken the structural integrity of the part and lead to increased sink-mark depth.

Fiber-Matrix Separation

During mold filling, reinforcing fibers in SMC and BMC materials become oriented by the flow field. When the SMC or BMC material is flowing through an area with a substructure, such as a rib or boss, both fiber orientation and variations in fiber-resin content will develop. Thus, within the area of the rib entrance, there will exist resin as well as fiber enriched areas. This fiber-resin content variation gives rise to variations in material properties, such as thermal and polymerization shrinkage coefficients, which are the two main causes of sink-mark formation.

So far, no theoretical model exists to predict the fiber-matrix separation during flow of reinforced resins. It is easy to see that both the resin and fiber flow together and are linked by a hydrodynamic interaction. However, external forces, fiber interaction, and mold geometry will cause the fibers to lag the flow of the resin.

To gain a basic understanding about the resin and fiber flow mechanism, a preliminary analysis was performed. First, Darcy's law was applied to the area at the rib entrance to solve for the resin flow out of the random fiber bed due to the pressure difference at the rib entrance. Darcy's law for flow through a porous or fibrous media can be written as

$$V^{D}_{resin} = -\frac{\underline{\underline{K}}}{\eta}\Delta P \tag{4}$$

where V^{D}_{resin} is the volume-average resin velocity, ΔP is the resin pressure, η is the resin viscosity and $\underline{\underline{K}}$ is the permeability of the porous media. Recently, Bakharev and Tucker [5] developed a micromechanical model for permeability of random fiber beds, using a self-consistent approach. The model predictions for in-plane permeability of a random fiber glass mat compared well to experimental results. Figure 5 presents the dimensionless permeability, K/r^2, as a function of fiber content, where r is a typical fiber radius [5].

By solving Darcy's law using the permeability data, the resin velocity flowing out of the fiber bed can be obtained.

When the SMC or BMC material is filling the mold cavity, the resin and the fibers are moving together, bounded by the hydrodynamic interaction. However, due to the pressure drop at the rib entrance, the resin flow out of the fiber bed will cause a fiber-matrix separation. A schematic of the material flow behavior at the rib entrance is shown in Fig. 6. Here Q^{D}_{resin} is the volumetric flow rate of the resin out of the fiber bed, and can be solved by Darcy's law. Q_{comp} indicates the volumetric flow rate of the composites into the rib section.

The volumetric flow rate of the fibers can be written as

$$Q_f = V_f A = \phi V_{comp} A \tag{5}$$

where V_f and V_{comp} are the velocity of the fibers and the velocity of the composite, respectively. A is the cross sectional area and ϕ is the volume fraction of the fibers in the SMC or BMC system being processed.

On the other hand, the volumetric flow rate of the resin can be represented as

$$Q^{tot}_{resin} = \left[(1-\phi)V_{comp} + V^{D}_{resin}\right]A \tag{6}$$

Performing a balance, after flow into the rib, including fiber-matrix separation, the new fiber content inside the rib ϕ_N is represented as

$$\phi_N = \frac{\phi V_{comp}}{V_{comp} + V^{D}_{resin}} \tag{7}$$

From Eq. (7) we can see that when $V^{D}_{resin}=0$, no resin is being squeezed out of the fiber bed and the new fiber content coefficient is equal to the original fiber volume fraction of the composite system. With an increase in the

amount of resin flow from the fiber bed at the rib entrance, the fiber content in the rib will drop.

The ratio of ϕ_N to ϕ is plotted in Fig. 7 with respect to the ratio of rib thickness to flange thickness, L/H, and with respect to the ratio of rib entrance radius to flange thickness, R/H. Figure 7 shows that when the rib thickness and lead-in radius are small, the value of ϕ_N/ϕ is small, indicating there is less fibers in the rib. With increasing rib thickness or lead-in radius, the new fiber content coefficient approaches the original fiber volume fraction, thus indicating less fiber-matrix separation.

Experimental Results

To test the plausibility of our model we measured the fiber density in a section of a typical compression molded SMC part (Fig.8). The fiber density distribution was determined using burn-out tests. Figure 8 shows the average fiber content by weight in the subsections labeled A through F. The fiber density was measured in each of the smaller subdivisions shown in the figure. The weight of each sample was recorded before (m_s) and after (m_a) the burn-out test. Since the organic portions of the resin will completely burn-out and 44% of the calcium carbonate will also disappear we can determine the fiber content in the sample using

$$\phi_N = 1 - \left(\frac{1+\kappa}{1+0.44\kappa}\right)\frac{\Delta m}{m_s} \qquad (8)$$

where $\Delta m = m_s - m_a$ and κ the ratio of mineral to organic mass content in the resin. The filtering effect that the fiber bed has on the calcium carbonate filler during flow is neglected, thus, κ can be assumed to be constant throughout the process.

The measured fiber content inside the rib was much lower than the rest of the part. This is in agreement with the model predictions. In addition, a lower fiber density was found in sections A and B, resulting from the resistance as the material moved past the sharp corner. Similar analysis, as performed on the ribbed sub-section, can be done on other typical geometries found in fiber reinforced composite parts.

Acknowledgments

The authors would like to acknowledge the Square D Company and The Budd Company for their financial support.

References

1. Jutte, R.B., International Automotive Engineering Conference, ASME 730171, (1973).
2. Sun, E.S., *Ph.D. Thesis*, University of Wisconsin-Madison, 1996.
3. Osswald, T.A., *Ph.D. Thesis*, University of Illinois at Urbana-Champaign, 1986.
4. Michaeli, W., and E. Semmler, Unpublished research, IKV-Aachen, (1996).
5. Bahharev, A.S. and C.L. Tucker II, SPE ANTEC, 797, (1996).

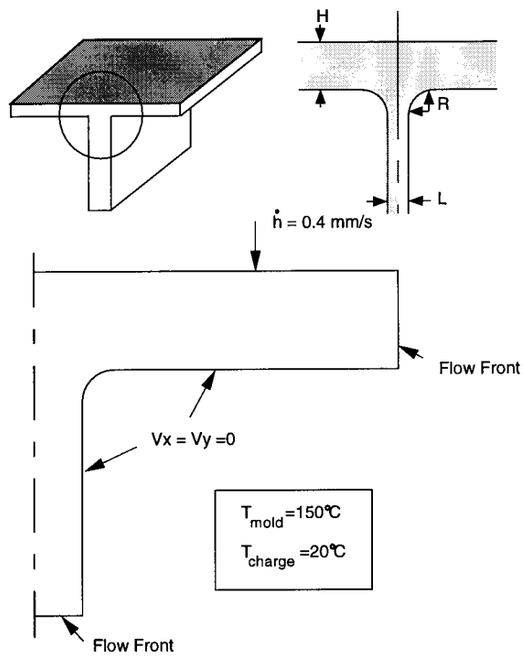

Figure 1. Nomenclature and boundary conditions.

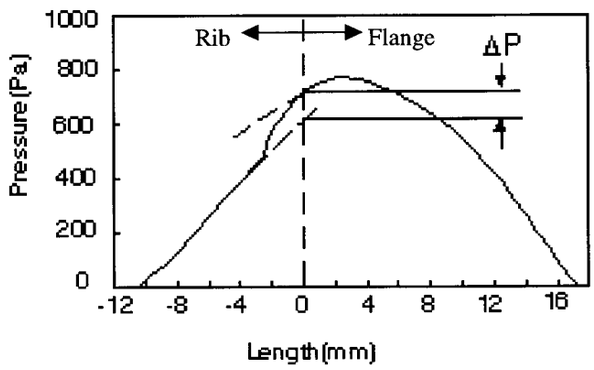

Figure 2. Pressure drop at the rib entrance area.

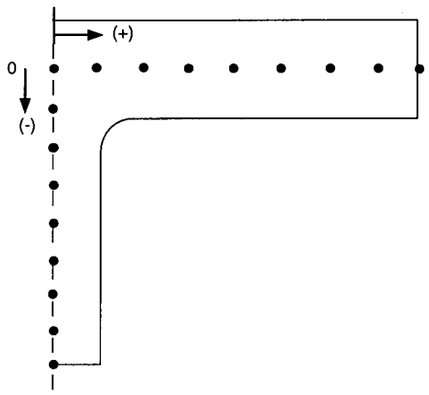

Figure 3. Schematic of the pressure distribution points used for plotting.

$$\Pi_1 = \frac{\Delta P\, H}{\eta \dot{h}}$$

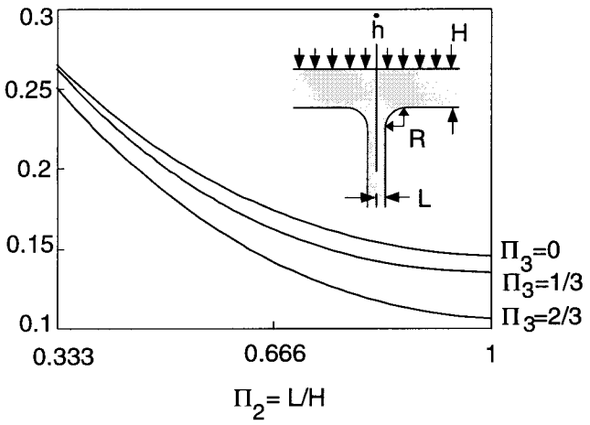

Figure 4. Relationship of the three dimensionless parameters for flow into ribbed the ribbed section.

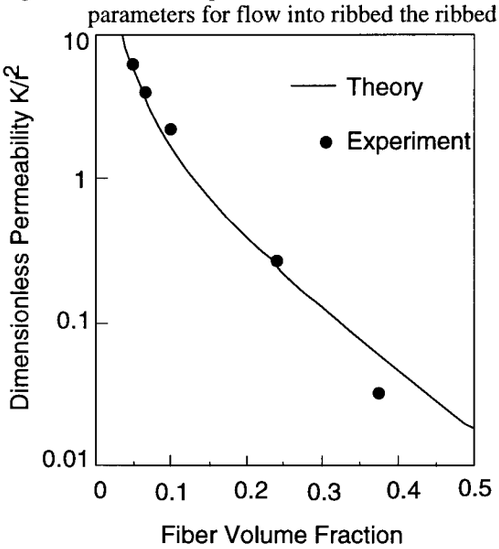

Figure 5. Model predictions compared to experiments for the permeability of random fiber mats.

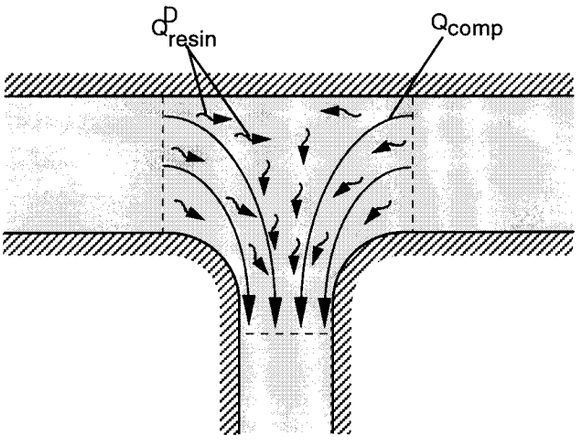

Figure 6. Schematic of the material flow behavior at the rib entrance.

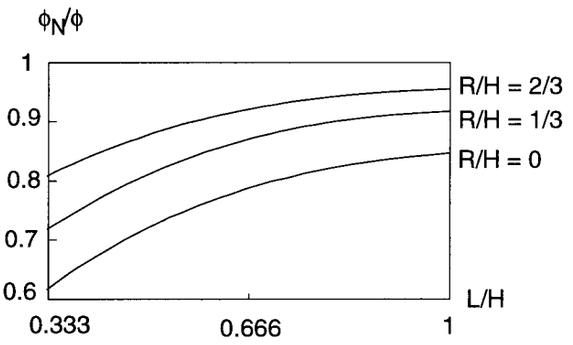

Figure 7. Relationships of ϕ_N/ϕ and geometric and processing conditions.

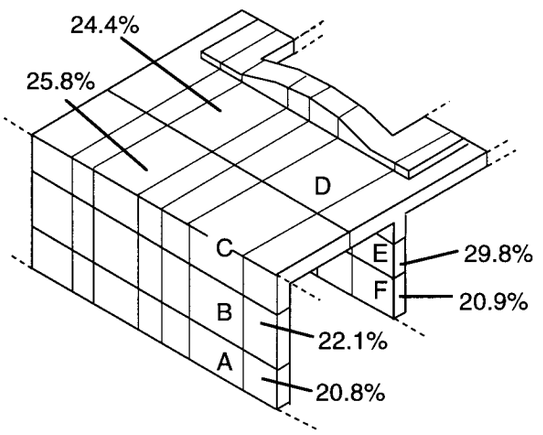

Figure 8. Fiber density distribution for sample sections.